Realizing ultrahigh ZT value and efficiency of the Bi₂Te₃ thermoelectric module by periodic heating

Ding Luo[a,b*], Ying Li[c], Yuying Yan[c], Xiaoming Hu[d], Xi'an Fan[d], Wei-Hsin Chen[e,f,g], Yong Ren[h], Bingyang Cao[b],

[a] College of Electrical Engineering & New Energy, China Three Gorges University, Yichang 443000, China

[b] Key Laboratory for Thermal Science and Power Engineering of Ministry of Education, Department of Engineering Mechanics, Tsinghua University, Beijing 100084, China

[c] Faculty of Engineering, University of Nottingham, University Park, Nottingham NG7 2RD, UK

[d] The State Key Laboratory of Refractories and Metallurgy, Wuhan University of Science and Technology, Wuhan 430081, China

[e] Department of Aeronautics and Astronautics, National Cheng Kung University, Tainan 701, Taiwan

[f] Research Center for Smart Sustainable Circular Economy, Tunghai University, Taichung 407, Taiwan

[g] Department of Mechanical Engineering, National Chin-Yi University of Technology, Taichung 411, Taiwan

[h] Key Laboratory of Carbonaceous Wastes Processing and Process Intensification Research of Zhejiang Province, University of Nottingham Ningbo China, Ningbo 315100, China

*Corresponding authors: Ding_L@outlook.com

Abstract: Thermoelectric power generation is regarded as a promising technology to convert waste heat into electricity. This study aims to address the low conversion efficiency of thermoelectric modules and introduces a novel periodic heating method to enhance their performance. Two new indicators, time average ZT_{ta} value and effective conversion efficiency, are introduced to assess the dynamic behavior of thermoelectric modules. A Bi₂Te₃-based thermoelectric module with n-type Bi₂Te₃₋ₓSeₓ and p-type BiₓSb₂₋ₓTe₃ materials is adopted as the research objective and tested on a designed transient experimental setup. Besides, a transient numerical model is developed to explore the optimal transient heat source and study the effect of various parameters on dynamic behavior. Compared with the steady-state efficiency of 3.76% and ZT_{ta} value of 0.78 at a heat supply of 60 W, the time average efficiency and ZT_{ta} value are improved by 52.93% and 43.59% respectively using the periodic heating method. Also, a smaller leg height, a larger leg area, more TE couples, and lower thermal conductivity are suggested for improving the dynamic behavior. This work offers a new periodic heating method to improve the output performance of thermoelectric modules, which may promote the broader application of thermoelectric power generation technology.

Keywords: thermoelectric generator; dynamic behavior; periodic heating; conversion efficiency

1. Introduction

Thermoelectric (TE) technology has gained great attention in the field of waste heat recovery because of its ability to directly convert heat into electricity [1, 2]. As a solid-state energy converter, the TE module was incorporated into heat exchangers to harvest waste heat from automobile engine [3-5], industrial exhaust [6, 7], ship engine [8, 9], etc. However, the low conversion efficiency of TE modules hampers their commercial applications in the field of waste heat recovery. Numerous efforts have been made for the structural optimizations of TE modules and thermoelectric generator (TEG) systems to enhance the conversion efficiency, such as segmented [10], U-type [11], Y-type [12] TE modules, and converging [13], metal foam [14], heat pipe [15] TEG systems. By employing these optimization techniques, the TE conversion efficiency has been improved to a certain extent. Besides, the TE module was used as a power source in some fields to provide electrical energy, such as solar power generation [16], wearable devices [17], and spacecraft [18]. With the improvement of conversion efficiency, TE modules are expected to achieve more widespread applications.

In addition to structural optimization, another effective way to improve conversion efficiency is to improve the figure-of-merit (*ZT*) value of thermoelectric materials. At present, compared with high-

or medium-temperature thermoelectric materials [19-21], the Bi_2Te_3-based materials are more widely used and successfully commercialized, as their high ZT value of about 1 at room temperature. However, to achieve a wide range of industrial applications, the ZT value is expected to break through the threshold of 2 [22]. In this regard, the nanocomposite technology has been intensively investigated as it can significantly improve the ZT value by adjusting the electron and phonon transport and energy band structure of materials at the micro-level. For example, nanocrystals allowed the p-type $Bi_xSb_{2-x}Te_3$ bulk materials to reach a peak ZT of 1.4 at 373 K [23] through phonon scattering. In Ref. [24], an ultrahigh ZT of 1.86 at 320 K was observed for p-type $Bi_{0.5}Sb_{1.5}Te_3$ bulk materials by embedding dense dislocation arrays into grain boundaries. Zhuang et al. [25] fabricated a p-type $(Bi, Sb)_2Te_3$-based module with a ZT value of 1.55 at 348 K by incorporating a mixture of BiI_3 and Zn at the nanoscale into the alloy, and a TE conversion efficiency of 5.2% is measured. Accordingly, the conversion efficiency of TE modules can be effectively improved by enhancing the ZT value of TE materials with nanocomposite technologies. However, the commercialization of these nanostructured TE materials is hampered due to the high cost and difficulty in maintaining stable high performance in their mass production.

In order to improve the conversion efficiency of TE modules, this work aims to explore a new performance improvement method from the perspective of heat sources, rather than from the perspective of structural and material optimizations mentioned above. In previous literature, the ZT value and efficiency of TE modules were tested under steady-state conditions. Nevertheless, heat sources are not always constant in practical applications, i.e., solar heat is weather-dependent and automobile exhaust heat depends on driving cycles. Under transient temperature excitations, the dynamic performance of TE modules is different from that under steady-state conditions due to the influence of thermal inertia [26]. After a period of heating, even if the heating is stopped, the TE module could continue to work until the hot-side temperature drops to equal the cold-side temperature. Therefore, this phenomenon can be used to boost the performance of the TE module by applying a transient heat source on its hot side, and the authors in Refs [27, 28] have already analyzed the feasibility of improving the output performance of the TE module with transient heat sources from a theoretical perspective.

In this study, we report a periodic heating method for Bi_2Te_3 TE modules to reach an ultra-high performance. The effective efficiency (η_{eff}) and time average ZT value (ZT_{ta}) were proposed to estimate the dynamic performance of the TE module within a certain period. Compared with traditional steady-state efficiency and ZT value, they can more accurately reflect the performance of TE modules under

actual transient conditions. Firstly, a Bi_2Te_3 TE module was constructed and used as the research objective, where the $Bi_2Te_{3-x}Se_x$ materials synthesized by the hot pressing method and $Bi_xSb_{2-x}Te_3$ materials by alloy melting and spark plasma sintering methods are used as n-type and p-type legs, and copper sheets and Al_2O_3-based ceramic are used as electrodes and substrates, respectively. Furthermore, a transient experimental bench was designed to validate the proposed concept. Finally, with the consideration of thermal-electric coupling effects, we developed a 3D transient thermal-electric numerical model to explore the optimal transient heat source and study the effect of various parameters on the dynamic behavior of the TE module.

1.1 Motivation for conducting this research

In previous studies [26, 29], it was observed that the average transient efficiency of TE modules under specific transient heat sources surpasses the steady-state efficiency. Upon deeper analysis of the underlying causes of this phenomenon, it was identified that it predominantly results from the periodic variations in the transient heat source. Therefore, this work tries to figure out how periodic heating enhances the dynamic performance of TE modules and which parameters influence this phenomenon. Based on the findings, a periodic heating method is suggested to improve the performance of the TE module, and detailed influential factors on it are introduced.

2. Principle of the improved efficiency and ZT value by periodic heating

This section mainly introduces two new indicators for evaluating dynamic behavior and the essence of why periodic heating can improve the performance of TE modules. Generally, a TE module is comprised of a string of p- and n-type semiconductor legs, metal conductive sheets, and insulating plates (Fig. 1a). The performance of TE materials determines the overall module performance. For an ideal TE module, the heat-to-electricity conversion efficiency can be expressed as [30]:

$$\eta_{\text{ideal}} = \frac{T_h - T_c}{T_h} \frac{\sqrt{1+ZT}-1}{\sqrt{1+ZT}+\frac{T_c}{T_h}} \tag{1}$$

with T_h and T_c being the hot- and cold-side temperatures of the TE module. For Bi_2Te_3-based materials, the ideal working temperature is about 500 K on the hot side and 300 K on the cold side. Under this condition, the maximum conversion efficiency is about 8.2% for the *ZT* value of 1.0 with commercial synthesis methods [31] and 12.0% for the *ZT* value of 1.86 with advanced nanotechnologies [24]. However, there is a great performance deterioration from the material level to the module level because of the thermal resistance of metal sheets and insulating plates and the energy loss caused by interfaces between different components. In practical situations, the conversion efficiency of TE modules is defined as

$$\eta_{\text{TEM}} = \frac{P}{Q_{\text{h}}} \tag{2}$$

where, P and Q_{h} are the power generation and heat absorption of the TE module. According to Eq. (2), conversion efficiencies of TE modules, η_{TEM}, at 6.0% (nanostructured Bi_2Te_3-based materials with a ZT of 1.4 and a ΔT of 217 K) and 4.83% (commercial Bi_2Te_3-based materials with a ZT of 1.0 and a ΔT of 200 K) were observed in labs [32] and commercial applications [29], respectively. Obviously, the actual conversion efficiency η_{TEM} is lower than the ideal efficiency η_{ideal}.
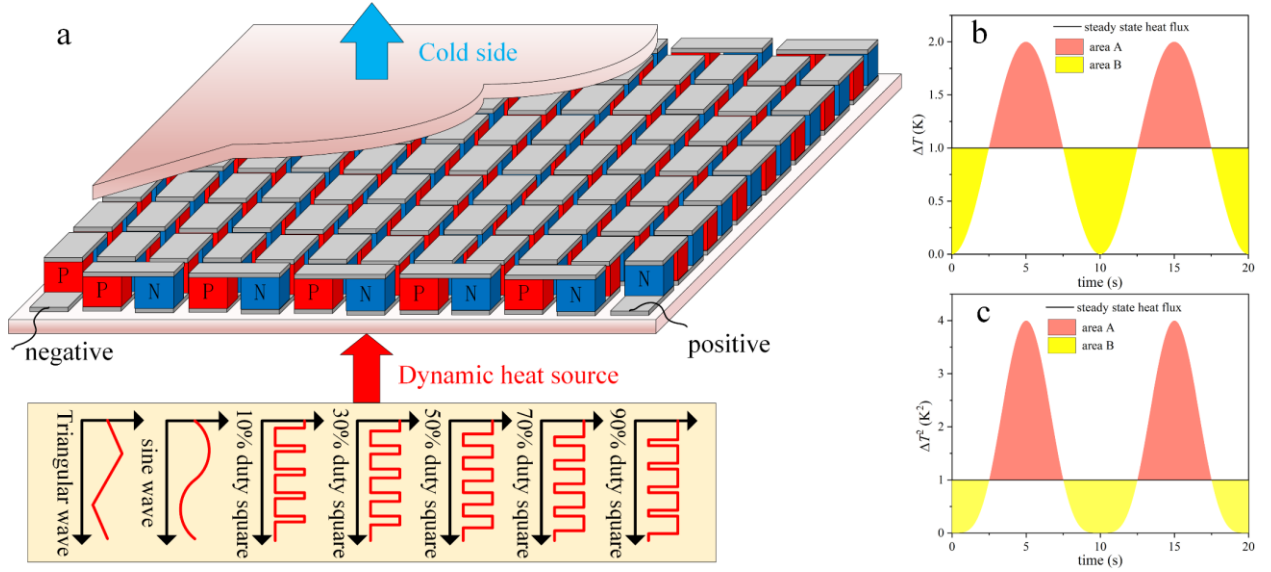
Fig. 1. Basic of dynamic heat sources applied to the TE module. a, Structure and working principle of the TE module. **b**, ΔT as a function of the sine wave and steady-state heat flux. **c**, ΔT^2 as a function of the sine wave and steady-state heat flux.

It should be noted that the above-mentioned performance indicators are described under the steady state. Considering that heat is usually not static in practical applications, two new indexes to characterize the behavior of TE modules under transient conditions are proposed in this work. They are the effective conversion efficiency (η_{eff}) and the time average ZT value (ZT_{ta}), which are defined as follows

$$\eta_{\text{eff}} = \frac{\int_0^{t_1} P(t)dt}{\int_0^{t_1} Q_{\text{h}}(t)dt} \tag{3}$$

$$ZT_{\text{ta}} = \left(\frac{T_{\text{h}} - T_{\text{c}} + \eta_{\text{eff}}T_{\text{c}}}{T_{\text{h}} - T_{\text{c}} - \eta_{\text{eff}}T_{\text{h}}}\right)^2 - 1 \tag{4}$$

where, t_1 is the time span of the transient heat source, $P(t)$ and $Q_{\text{h}}(t)$ are the transient output power and conversion efficiency of the TE module. Compared with the ZT value of TE materials, that is $ZT = S^2\sigma T/\lambda$, where S, σ, and λ represent Seebeck coefficient, the electrical and thermal conductivity

1 of TE materials, respectively, ZT_{ta} indicates the dynamic figure of merit of TE modules. In a steady

2 state, ZT_{ta} is lower than ZT, while in a transient state, ZT_{ta} may be larger than ZT due to the performance

3 enhancement by the transient heat source.

4   Transient heat sources, particularly periodic ones, are proven to be conducive to improving the

5 performance of TE modules [33]. The output power of the TE module can be expressed as [30]

$$P = \left(\frac{S\Delta T}{R_{in}+R_L}\right)^2 R_L \tag{5}$$

7 where R_{in} and R_L represent the internal and external resistances, respectively.
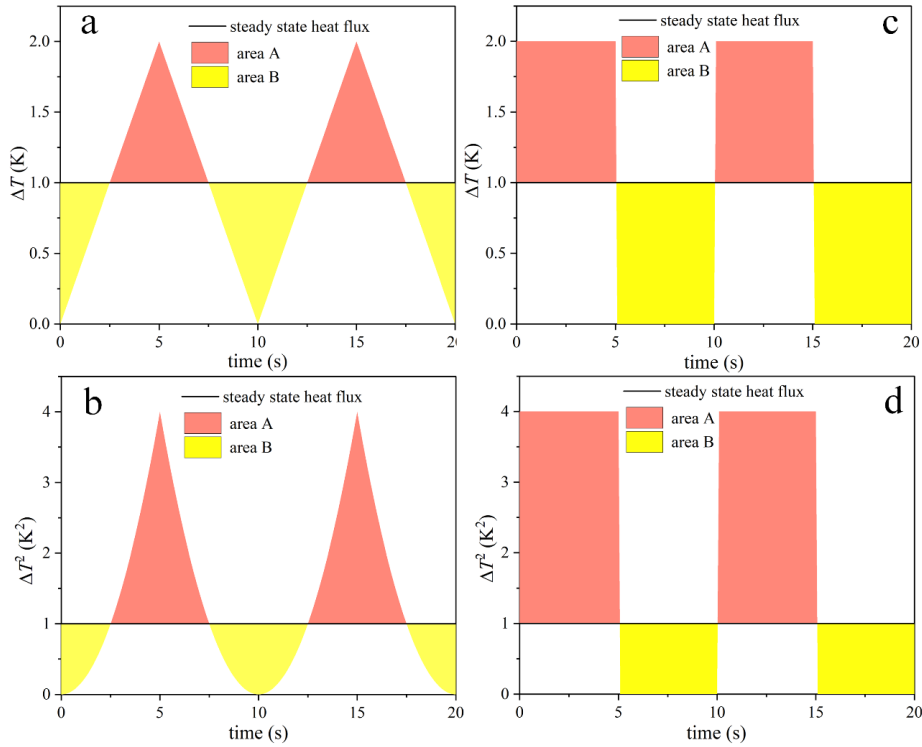
Fig. 2. a, ΔT as a function of triangular wave and steady-state heat flux. **b**, ΔT^2 as a function of triangular wave and steady-state heat flux. **c**, ΔT as a function of square wave and steady-state heat flux. **d**, ΔT^2 as a function of square wave and steady-state heat flux.

12   Combined with Eq. (2), it is obvious that the conversion efficiency is proportional to ΔT^2, instead

13 of ΔT. Compared with steady-state heat flux, for a given periodic heat flux, like a sine wave, the

14 corresponding changes from ΔT to ΔT^2 are shown in Fig. 1b and Fig. 1c, respectively. In Fig. 1c, the

15 difference between area A and area B indicates the ability of periodic heat sources to improve dynamic

16 performance. Comparing this enhancement ability of sine wave heat flux with those of triangular and

17 square wave ones (Fig. 2), it seems that the square wave is superior to the other two transient heat

18 sources because of its largest difference between area A and area B. To explore the optimal transient

1 heat flux, the dynamic response characteristics of the TE module under different waveform heat

2 sources are analyzed, including sine wave, triangular wave, and square wave. In addition, the influence

3 of different waveform parameters on η_{eff} and ZT_{ta} is studied, including amplitude, initial state, cycle

4 period, and duty ratio.

5 **3. Experimental setup**

6   In this section, to demonstrate the effectiveness of the periodic heating method in improving the

7 performance of TE modules via experiments, a transient test bench was designed. However, due to the

8 limitations of transient heat sources during experiments, it was planned to further explore the optimal

9 transient heat source through numerical models in the following section. Considering the significant

10 impact of contact thermal and electrical resistances on the performance of TE modules, to ensure the

11 accuracy of the numerical model, the designed bench was also used to examine the contact thermal

12 and electrical resistances of the TE module. This section provides a detailed introduction to the

13 experimental setup and measurement methods for contact thermal and electrical resistances.

14 *3.1 Test rig and experimental results*
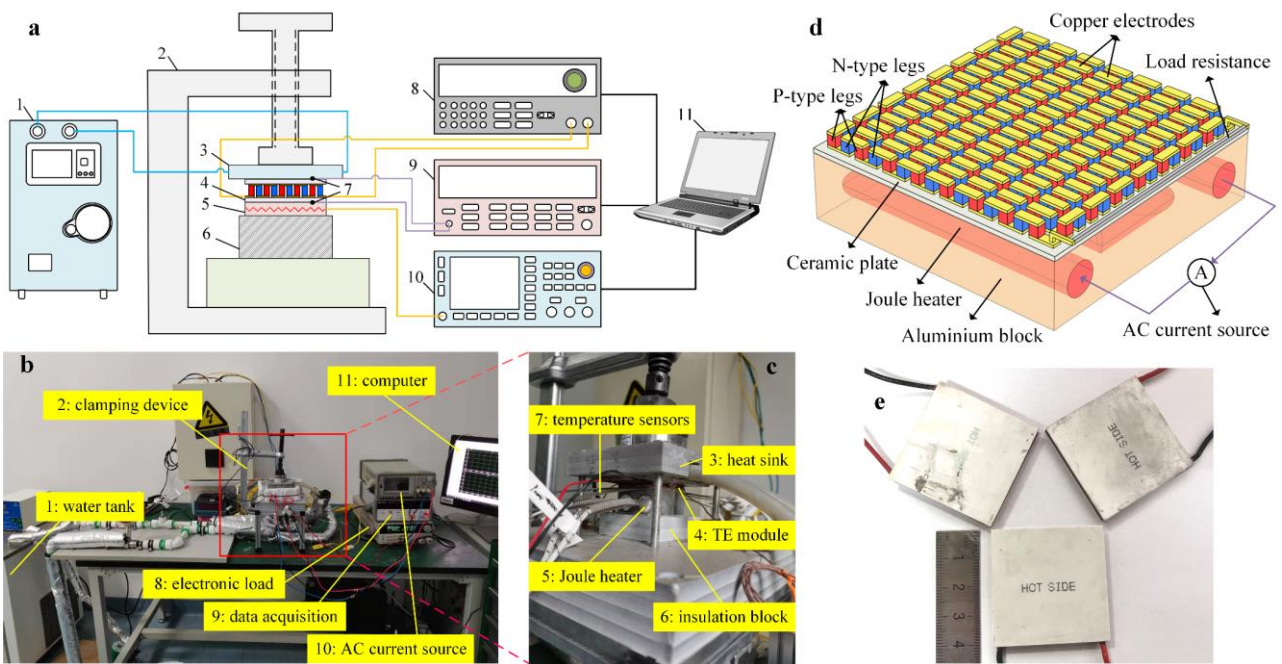
16 **Fig. 3. Experimental setup. a**, Schematic diagram of the test bench [29]. **b**, Actual picture of the whole test bench [29]. **c**,

17 Details of the TE module installation. **d**, Schematic diagram of the TE module and heat source. **e**, The fabricated TE

18 module.

19   Fig. 3 shows details of the transient experimental bench used to test the dynamic performance of a

20 TE module under different transient heat fluxes. A TEG1-12708 TE module was fabricated and used

as the research objective (Fig. 3e), which is provided by the company of Prof. Fan (Sagreon Corp., Hubei, China). It is composed of 127 pairs of TE legs, 254 copper electrodes, and two alumina ceramic plates, where the n-type $Bi_2Te_{3-x}Se_x$ materials are made by hot pressing (HP) method and p-type $Bi_xSb_{2-x}Te_3$ materials are made by alloy melting (AM) and spark plasma sintering (SPS) methods. Table 1 gives the detailed parameters of the TE module. To provide transient heat sources for the TE module, a Joule heater, powered by an AC current source, was inserted into the aluminum block. This block was applied to the hot side of the TE module (Fig. 3d). To avoid heat loss, an insulation block was padded at the bottom of the aluminum block (Fig. 3c). For the cold side, a water-cooled aluminum heat sink was applied on the top of the TE module (Fig. 3a and 3b). Driven by the water bath, the cooling water flowed through the heat sink to dissipate heat. Temperature sensors were attached to the top of the aluminum block, the hot side of the TE module, and the cold side of the TE module to measure the temperature of the heat source, the hot side, and the cold side of the TE module, respectively. Also, temperature sensors were connected to the data acquisition to read and record temperature signals. To test the electrical output performance of the TE module, an electronic load was set to be connected with its positive and negative poles. During steady-state experiments, it was found that the optimal load resistance is about 2 Ω. For this reason, the electronic load is set to 2 Ω during the transient test. To facilitate signal control and processing, the AC current source, data acquisition, and electronic load were connected to a computer to realize the mutual interaction of signals. The whole test rig was clamped together by a clamping device, and the thermal grease with a thermal conductivity of 6 $W \cdot m^{-1} \cdot K^{-1}$ was applied to the interfaces to eliminate the air gap between different components. Besides, the whole test system was wrapped with an aerogel blanket to reduce heat loss. Details about the test apparatus can be found in Table 2, including type, manufacturer, accuracy, and key parameters.

**Table 1.** Datasheet of the TEG1-12708 module.

Name	p-type thermoelectric leg	n-type thermoelectric leg	Copper electrodes	Ceramic plate
Thermal conductivity ($W \cdot m^{-1} \cdot K^{-1}$)	$1.6848 \times 10^{-7}T^3 - 1.8949 \times 10^{-4}T^2 + 0.0697T - 6.8387$	$1.4735 \times 10^{-7}T^3 - 1.5903 \times 10^{-4}T^2 + 0.0571T - 5.0958$	400	$-0.02857T + 28.3757$
Seebeck coefficient ($\mu V \cdot K^{-1}$)	$1.3222 \times 10^{-5}T^3 - 0.0171T^2 + 7.3095T - 853.6610$	$-1.5235 \times 10^{-5}T^3 + 0.0194T^2 - 8.2297T + 981.1090$	-	-
Electrical resistivity ($10^{-5}\Omega \cdot m$)	$-9.0350 \times 10^{-9}T^3 + 1.6380 \times 10^{-5}T^2 - 0.00425T + 0.6648$	$4.4520 \times 10^{-8}T^3 - 5.5288 \times 10^{-5}T^2 + 0.02591T - 3.4085$	1.67×10^{-3}	-
Specific heat ($J \cdot kg^{-1} \cdot K^{-1}$)	$1.7289 \times 10^{-5}T^3 - 0.0209T^2 + 8.4401T - 945.6858$	$1.0197 \times 10^{-5}T^3 - 0.0128T^2 + 5.3717T - 581.5998$	385	850
Density ($kg \cdot m^{-3}$)	6780	7800	8960	3600

Height (mm)	1.6	1.6	0.4	0.7
Area (mm^2)	1.4×1.4	1.4×1.4	1.4×3.8	40×40
Number	127	127	256	2

Table 2. Details about the test apparatus.

Name	Type	Manufacturer	Accuracy	Key parameters
Joule heater	Iron	Xincheng, China	-	167 Ω
AC current source	HCP1022	Henghui, China	-	Square wave and triangular wave
Electronic load	IT8500+	ITECH, China	±0.01%	-
Data acquisition	34970 A	Keysight, China	±0.015%	Number of channels: 8
Temperature sensor	SA1XL-K-SRTC	OMEGA, US	±0.4%	Maximum temperature: 315ºC; Response time: ≤0.15 s
Insulation block	40×40×40 mm^3	Amanda, China	-	Thermal conductivity: 0.3 W·m^{-1}·K^{-1}
Water tank	DC-0530	Blue Power, China	-	Flow rate: 10 L/min Temperature range: -5ºC -95ºC
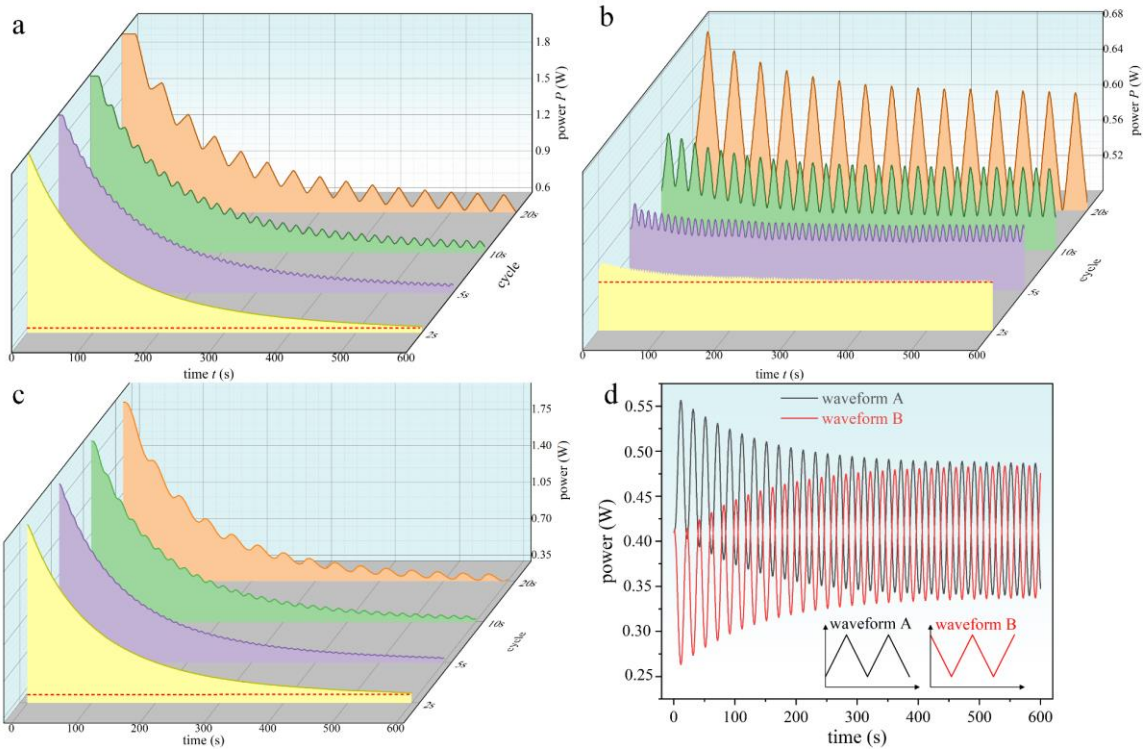
Fig. 4. Experimental results. a, Dynamic power under different square waves (initial state: Q_{max}). **b**, Dynamic power under different square waves (initial state: 50% Q_{max}). **c**, Dynamic power under different triangular waves (initial state: Q_{max}). **d**, Comparison of dynamic power between waveform A and waveform B.

Due to the limitation of the AC current source, with a maximum voltage of 80 V, the Joule heater can only provide the transient heat flux with square wave and triangular wave. According to the

1   resistance of the Joule heater, the maximum supplied heat (Q_{max}) for the TE module is about 32.32 W.

2   Therefore, the square wave transient heat fluctuates between 32.32 W and 0 W. The dynamic output

3   power of the TE module was observed under different square wave transient heat sources (Fig. 4a with

4   the initial state of Q_{max} and Fig. 4b with the initial state of 50% Q_{max}). The red dotted line in the figure

5   represents the steady-state output power under the heat input of 50% Q_{max}. The area above the red

6   dotted line represents the performance improvement by the square wave transient heat flux. Through

7   the comparison of Figs 4a and 4b, it can be obtained that the initial state plays an important role in the

8   dynamic behavior of the TE module. The higher the initial state level is, the greater the performance

9   improvement of the TE module can be achieved. Besides, the results of dynamic output power under

10   different cycle periods show that the cycle period does not affect performance enhancement but affects

11   the amplitude of fluctuation and the time required to reach a stable periodic output. When the periodic

12   heat stops, the output power will drop rapidly to 0. However, the periodic heat can prolong the decrease

13   process, which is the essence of performance improvement by periodic heating.

14   Compared with the square wave, the dynamic output power under the triangular wave transient heat

15   source varies with a smoother fluctuation (Fig. 4c). Similarly, the area above the red dotted line

16   represents the performance improvement. According to Fig. 2, a square wave is superior to a triangular

17   wave, bringing a higher dynamic performance. Compared with Fig. 4c, the output power in Fig. 4a

18   still does not reach a stable periodic output. Thus, it is difficult to distinguish the specific difference in

19   performance enhancement between square wave and triangular wave from Figs 4a and 4c. Therefore,

20   in the next section, we propose a comprehensive 3-D transient numerical model for the TE module to

21   explore the optimal transient heat source and its corresponding parameters. It should be noted that for

22   each type of transient wave, there exist two kinds of waveform: one is first rising and then falling

23   (waveform A) and the other is opposite (waveform B). Take the initial state of 50% Q_{max} under a

24   triangular wave as an example, we experimentally compared the dynamic output power of the TE

25   module under waveform A and that under waveform B (Fig. 4d). Obviously, waveform A can amplify

26   the performance of the TE module, but waveform B may deteriorate the performance. Therefore, the

27   transient heat sources in the following studies are all based on waveform A.

28   *3.2 Test of the interface contact resistances*

29   The interface contact has a significant influence on the performance of the TE module [10, 34]. To

30   ensure the accuracy of numerical simulations, the contact thermal and electrical resistances of the

31   module were measured experimentally. The contact electrical resistance exists on interfaces between

32   TE legs and connectors, and the contact thermal resistance exists on the interfaces between the heater

1 (or heat sink) and the TE module, between insulating plates and connectors, and between TE legs and

2 connectors, as shown in Fig. 5. Here, the contact thermal resistance between the heater (heat sink) and

3 the TE module was defined as the external contact thermal resistance, and others were assumed to be

4 the internal contact thermal resistance between insulating plates and connectors.

:thermal contact resistance
:electrical contact resistance
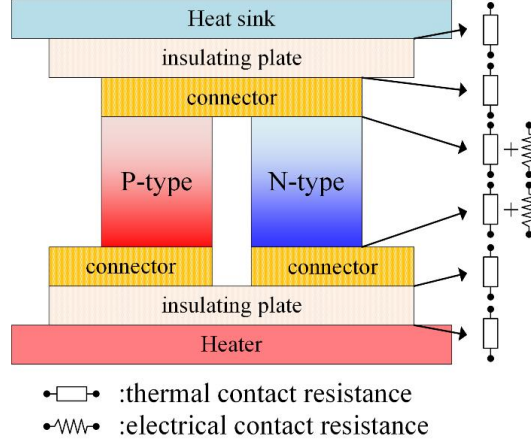
5

6 **Fig. 5.** Schematic diagram of the thermal and electrical contact resistances.

7 3.2.1 Thermal contact resistance

8 Based on the test rig in Fig. 3, we added an aluminum block to the hot side of the TE module to

9 measure the heat flux through the entire module, as shown in Fig. 6a. Here, three holes were drilled

10 inside the aluminum block to measure the temperature at the corresponding locations. The temperature

11 data required for calculating the contact thermal resistance include: T_b, T_m, and T_u for the measured

12 temperatures at the bottom, middle, and upper of the aluminum block, respectively; T_h for the

13 temperature at the top of the metal block; T_{h_ce} for the temperature of the contact surface between the

14 hot-side ceramic plate and the heat source; T_{c_ce} for the temperature of the contact surface between the

15 cold-side ceramic plate and the cooling source; and T_c for the temperature of the cooling source. Based

16 on the measured temperature data, the heat flux Q_h can be expressed as:

17
$$Q_h = \lambda_{al} \frac{A_{al}}{d_2}(T_u - T_h) - \frac{d_2(Q_{h1} - Q_{h2})}{2d_1} \tag{6}$$

18 with

19
$$Q_{h1} = \lambda_{al} \frac{A_{al}}{d_1}(T_b - T_m) \tag{7}$$

20
$$Q_{h2} = \lambda_{al} \frac{A_{al}}{d_1}(T_m - T_u) \tag{8}$$

21 where, λ_{al} and $A_{al} = 40 \times 40\ mm^2$ are respectively the thermal conductivity and cross-sectional area

22 of the aluminum block; $d_1 = 15$ mm represents the distance from the bottom hole to the middle hole

23 or from the middle hole to the upper hole of the aluminum block; $d_2 = 5$ mm represents the distance

from the upper hole to the top surface of the aluminum block. Considering the heat loss from the aluminum block to the environment, a correction term is incorporated into the formula to ensure the accuracy of the calculated heat flux, as shown in the last term of Eq. (6), which represents the heat loss from the upper hole to the top surface of the aluminum block.
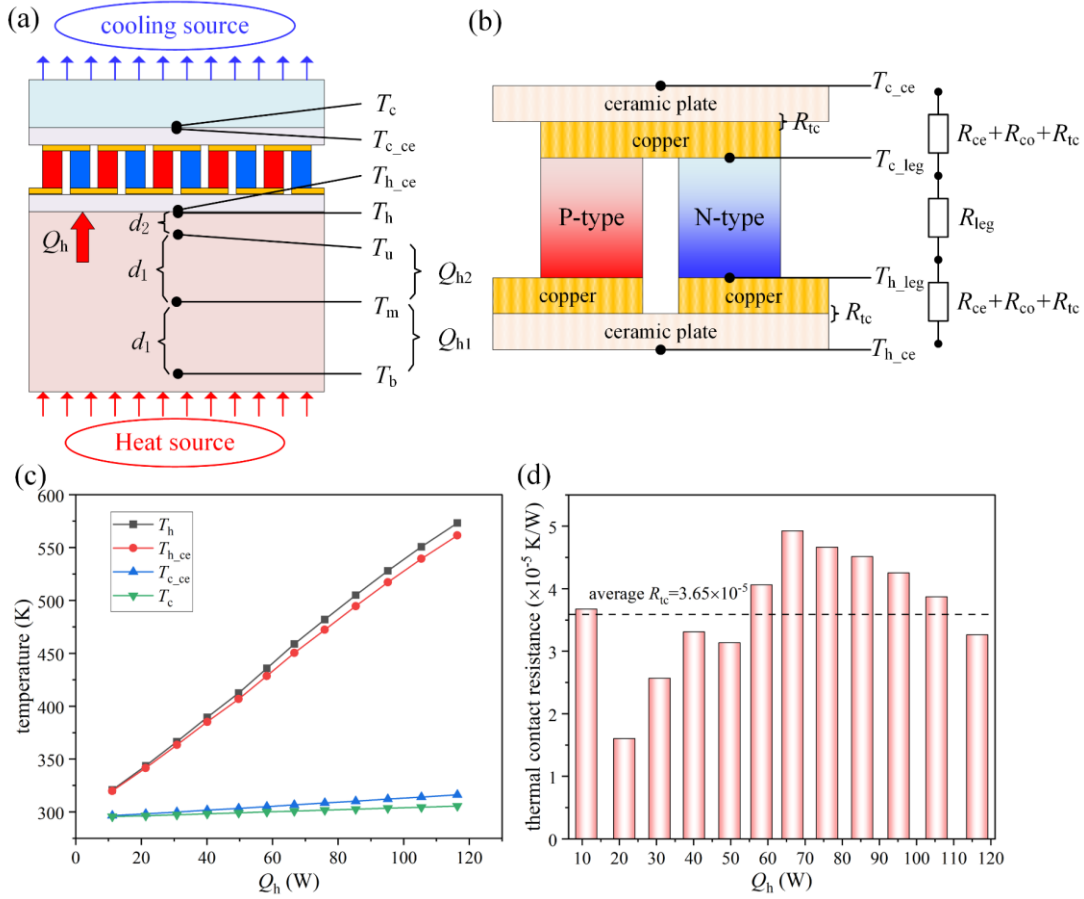
Fig. 6. Principle and results of the thermal contact resistance. **a**, Diagram of the test system. **b**, Thermal resistance network of the TE module. **c**, Test results. **d**, Calculated results of the contact thermal resistance.

The schematic diagram of the thermal resistance network is presented in Fig. 6b, where R_{tc_h} and R_{tc_c} denote the external hot- and cold-side contact thermal resistances of the module (not shown in the figure), respectively; R_{tc} represents the internal contact thermal resistance of the module. Even though R_{tc} is defined as the interface between copper electrodes and ceramic plates, it takes into account the effect of the contact thermal resistance between thermoelectric legs and copper electrodes, thereby ensuring high accuracy of the results.

R_{tc_h} and R_{tc_c} can be calculated from Q_h, T_h, T_{h_ce}, T_{c_ce}, and T_c:

$$R_{tc\_h} = \frac{T_h - T_{h\_ce}}{Q_h} \tag{9}$$

12

$$R_{\text{tc\_c}} = \frac{T_{\text{c\_ce}} - T_{\text{c}}}{Q_{\text{h}}} \tag{10}$$

And R_{tc} can be expressed by:

$$R_{\text{tc}} = \frac{1}{2}\left(\frac{T_{\text{h\_ce}} - T_{\text{c\_ce}}}{Q_{\text{h}}} - 2R_{\text{ce}} - 2R_{\text{co}} - R_{\text{leg}}\right) \tag{11}$$

with

$$R_{\text{leg}} = \frac{h_{\text{leg}}}{\left(\lambda_{\text{p}}(T) + \lambda_{\text{n}}(T)\right)NA_{\text{leg}}} \tag{12}$$

where R represents the thermal resistance. Subscripts ce, co, leg, p, and n represent ceramic plates, copper electrodes, thermoelectric legs, p-type thermoelectric legs, and n-type thermoelectric legs, respectively. N, h, A, and λ are respectively the number, height, area, and thermal conductivity of p-type or n-type thermoelectric legs.

The thermal contact resistances R_{tc}, $R_{\text{tc\_h}}$, and $R_{\text{tc\_c}}$ are computed from the temperature test data of T_{b}, T_{m}, T_{u}, T_{h}, $T_{\text{h\_ce}}$, $T_{\text{c\_ce}}$, and T_{c}, along with the TEG1-12708 module datasheet (Table 1). Fig. 6c gives the temperature test results under different heat fluxes, while Fig. 6d shows the calculated results of the internal contact resistance R_{tc} ($R_{\text{tc\_h}}$ and $R_{\text{tc\_c}}$ not shown in this figure). Finally, after averaging the calculated results, we have $R_{\text{tc}} = 3.65 \times 10^{-5}$ m$^2\cdot$K/W, $R_{\text{tc\_h}} = 1.78 \times 10^{-4}$ m$^2\cdot$K/W, $R_{\text{tc\_c}} = 1.39 \times 10^{-4}$ m$^2\cdot$K/W.
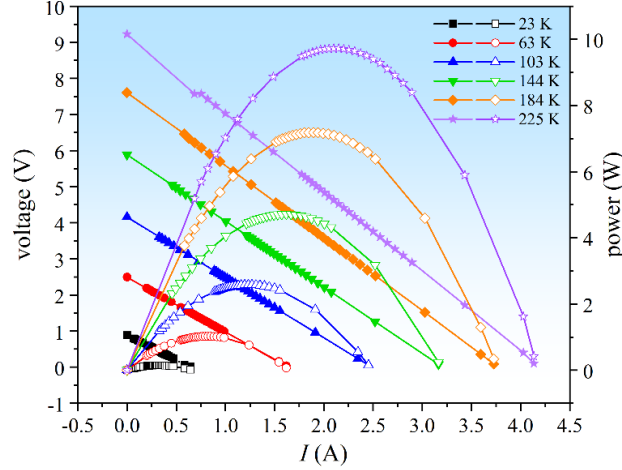
3.2.2 Electrical contact resistance

As for the electrical contact resistance R_{ec}, it can be regarded as the difference between the tested internal resistance of the TE module and calculated resistances of TE legs and copper electrodes, that is:

$$R_{\text{ec}} = R_{\text{test}} - \left(\sigma_{\text{p}}^{-1}(T) + \sigma_{\text{n}}^{-1}(T)\right)\frac{Nh_{\text{leg}}}{A_{\text{leg}}} - \sigma_{\text{co}}^{-1}\frac{2Nh_{\text{co}}}{A_{\text{co}}} \tag{13}$$

where R_{test} denotes the internal resistance value measured, which is determined using the slope of the voltage-current characteristic curve as the internal resistance of the TE module. σ^{-1} represents the electrical resistivity. The second and last terms on the right side of Eq. (13) represent the internal resistances of thermoelectric legs and copper electrodes respectively.

Fig. 7 shows the experimental results of the electrical contact resistance. As can be seen, the output power of the TE module has a parabolic relationship with the current, while the output voltage of the module linearly decreases with the increase of the current, and the absolute value of the slope of the U-I curve represents the module internal resistance R_{test}. Based on Eq. (13), the contact resistance at different temperatures can be calculated. The average value with different temperatures is finally obtained, that is $R_{\text{ec}} = 1.18 \times 10^{-10}\Omega\cdot$ m^2.

3.3 Measurement uncertainty analysis

In general, the uncertainty can be classified into two categories: Type A and Type B. Type A is related to random errors and can be estimated using statistical and repetitive methods, and Type B is related to systematic errors and can be obtained by looking up specific information of apparatus. In this research, there is no statistical analysis in reading the test data of measuring devices. Therefore, the uncertainties of experimental results are always Type B, which can be calculated from the following equation [35, 36]:

$$u = \frac{a}{\sqrt{3}} \tag{14}$$

where *a* is the accuracy of the instrument, and *u* is the standard uncertainty. The uncertainties associated with the experiments are given in Table 3.

Table 3. Standard uncertainties associated with measuring devices

Measuring device	Accuracy	Range	Standard accuracy
Electronic load	0.01% V	0-1000 V	0.006% V
Data acquisition	0.015% ᵒC	0-900 ᵒC	0.009% ᵒC
Temperature sensor	0.4% ᵒC	0-900 ᵒC	0.24% ᵒC

4. 3-D transient numerical modeling

In this section, to further explore the optimal transient heat source and investigate the dynamic behavior of the TE module, a 3-D transient thermal-electric numerical model for the whole TE module test system was established, and corresponding experimental verification was completed.

4.1 Governing equations and boundary conditions

To ensure the accuracy of the numerical model, the thermoelectric coupling effects of the TE module

1   have to be fully considered, including the Seebeck effect, Peltier effect, and Thomson effect. In general,

2   the conservation equations in a transient state of the whole TE system include:

$$(\rho c)_{\text{p,n}} \frac{\partial T}{\partial t} = \nabla \cdot (\lambda_{\text{p,n}} \nabla T) + \sigma_{\text{p,n}}^{-1}(T)\vec{J}^2 - T_{\text{p,n}}\vec{J} \cdot \nabla S_{\text{p,n}}(T) - \frac{\partial S_{\text{p,n}}(T)}{\partial T_{\text{p,n}}} T_{\text{p,n}}\vec{J} \cdot \nabla T \quad (15)$$

$$(\rho c)_{\text{co,L,h}} \frac{\partial T}{\partial t} = \nabla \cdot (\lambda_{\text{co,L,h}} \nabla T) + \sigma_{\text{co,L,h}}^{-1}(T)\vec{J}^2 \quad (16)$$

$$(\rho c)_{\text{ce,al}} \frac{\partial T}{\partial t} = \nabla \cdot (\lambda_{\text{ce,al}} \nabla T) \quad (17)$$

$$\vec{E} = -\nabla \varphi + S(T)\nabla T \quad (18)$$

$$\vec{J} = \sigma \vec{E} \quad (19)$$

$$\nabla \cdot \vec{J} = 0 \quad (20)$$

9   where, ρ, c, $\vec{J}$, $\vec{E}$, and φ represent the density, specific heat, current density vector, voltage density

10   vector, and electrical potential, respectively. Subscripts p, n, co, L, h, ce, and al represent the p-type

11   TE legs, n-type TE legs, copper electrodes, load resistance, Joule heater, ceramic plate, and aluminum

12   block, respectively. In Eqs (15)-(17), the first term on the left and right sides expresses the transient

13   term and Fourier heat conduction respectively. The last three terms in Eq. (15) from left to right express

14   the Joule heat, Peltier heat, and Thomson heat, respectively. The term of $S(T)\nabla T$ in Eq. (18) denotes

15   the Seebeck voltage. Eq. (20) represents the continuity of current. The 3-D geometrical model of the

16   TE test system created in the software had the same parameters as those in the experiment.

17   To solve the above differential equations, reasonable boundary conditions are essential. Herein, the

18   transient voltage input $U_{\text{in}}(t)$ was defined on one end of the Joule heater to provide transient heat flux

19   for the TE module. Based on this voltage input, the transient heat source energy provided for the TE

20   module can be estimated by $U_{\text{in}}^2(t)/R_{\text{h}}$, with R_{h} being the electrical resistance of the Joule heater. A

21   grounding boundary condition was defined on the other end of the Joule heater. For the boundary

22   conditions of the TE module, on the cold-side surface of the TE module, a constant temperature of 300

23   K was defined due to the use of a thermostat water bath. The contact interface between the negative

24   side of the TE module and the load resistance was grounded. On the surfaces of the aluminum block

25   except the one contacting the TE module, the adiabatic boundary condition was defined. In addition,

26   according to the test results of the interface contact resistance in Section 3.2, the interface boundary

27   conditions with electrical contact resistances of 1.18×10^{-10} $\Omega\cdot\text{m}^2$ and thermal contact resistance of

28   3.65×10^{-5} $\text{K}\cdot\text{m}^2\cdot\text{W}^{-1}$ were defined on interfaces between copper electrodes and TE legs, and between

29   ceramic plates and copper electrodes, respectively. Due to the use of thermal grease, thermal contact

30   resistances of 1.78×10^{-4} $\text{K}\cdot\text{m}^2\cdot\text{W}^{-1}$ and 1.39×10^{-4} $\text{K}\cdot\text{m}^2\cdot\text{W}^{-1}$ were defined on the hot and cold sides of

1 the TE module respectively. So far, the thermoelectric effect and Joule heating process in a transient

2 state were fully considered in the numerical model, which is consistent with the actual situation.

3 *4.2 Model validation*

4 **Table 4.** Grid independence analysis in a steady state of the TE module under a temperature difference of 200 K.

Grid name	Grid parameter	Grid number	Ouput voltage (V)	Error of voltage
Grid i	Coarse	63147	3.8973	0.10%
Grid ii	Standard	76476	3.8957	0.05%
Grid iii	Fine	94664	3.8947	0.03%
Grid iv	Relatively finer	160351	3.8936	NA

5 The 3-D transient distributions of $\vec{J}$, $\vec{E}$, and T are numerically solved using the finite element method

6 for space variables and the backward difference method for time variables on the platform of COMSOL

7 Multiphysics. Important value, $P(t)$, derived by $U_L^2(t)/R_L$, was calculated from $\vec{E}$. More precisely, the

8 output voltage U_L was estimated by an area integration of $\vec{E}$ over the selected cross section. Through

9 the grid independence analysis of the TE module in a steady state, as shown in Table 4, grid iii with

10 94664 grids was selected for the following investigations to make a tradeoff between accuracy and

11 calculation time. As for the time variable, the adaptive time step with a maximum limit of 0.1 s was

12 adopted to perform transient simulations. The 3-D transient numerical model was verified with our

13 experimental results, as illustrated in Fig. 8. Under the same working conditions, the simulation results

14 were in good agreement with the experimental results. Consequently, the developed model is capable

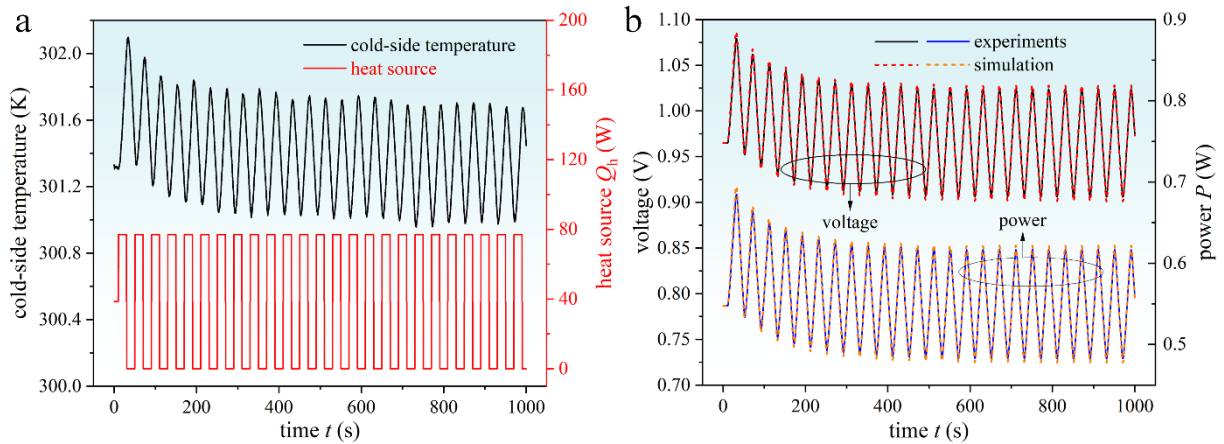15 of predicting the dynamic behavior of the TE module with high accuracy.

17 **Fig. 8.** Experimental validation. **a**, Experimental conditions including the transient heat generated by the Joule heater and
18 the cold-side temperature of the TE module. **b**, Comparison of transient voltage and power between experimental and
19 simulation results.

20 **5. Results and discussion**

16

1   Based on the developed numerical model, the detailed distribution characteristics of the TE module
2   with various variables were given in this section. In addition, the numerical model was used to explore
3   the optimal transient heat source and study the effects of different structural and material parameters
4   on the dynamic behavior of the TE module.

5   *5.1 Numerical Results*

6   Considering that the maximum working temperature of the TE module was about 500 K, which
7   corresponds to a maximum heat supply of 120 W, the transient heat source of the TE module was set
8   to fluctuate between $Q_h = 120$ W and $Q_h = 0$ W. Also, we compared the steady-state performance when
9    $Q_h = 60$ W with the transient performance when Q_h fluctuates (the average value was 60 W). Taking
10   the steady-state numerical results as an example, the distribution characteristics of different variables
11   of the TE module were described in detail, which contributes to understanding the interior behavior
12   better. The temperature distribution shows that the temperature drop from the heat source to the cold
13   side of the TE module mainly occurs on TE legs (Fig. 9a) because of the relatively low thermal
14   conductivity of TE materials. The temperature of the load resistance is the highest due to the Joule
15   heat, and its heat generation indicates the power generation of the TE module. The electrical potential
16   of the TE module increases with the series of TE legs (Fig. 9b), and its output voltage equals the
17   potential difference of the load resistance (herein is 2.13 V). According to Eqs (3) and (4), the
18   corresponding η_{eff} and ZT_{ta} in a steady state are 3.76% and 0.78, respectively. It should be noted that
19   the ZT_{ta} value of 0.78 for the TE module is lower than the ZT value of about 0.9 for TE materials
20   (calculated from material properties in Table 1) due to the performance deterioration from the material
21   level to the module level. However, ZT_{ta} in the transient state with periodic heat flux excitations may
22   be greater than the ZT value of its TE materials. The current density in p-type legs is opposite to that
23   in n-type legs due to the opposite current direction (Fig. 9c). Similarly, the current generated can be
24   estimated by an area integration of the current density over a selected cross section, which is 1.07 A
25   herein. Also, the distribution of the ZT value along TE legs can be estimated by the numerical model
26   (Fig. 9d). As the ZT value is proportional to the absolute temperature, it decreases from the hot side to
27   the cold side of the TE legs due to the decrease of the local temperature. The ZT value of p-type legs
28   is greater than its n-type counterparts due to the superior performance of the p-type Bi_2Te_3-based
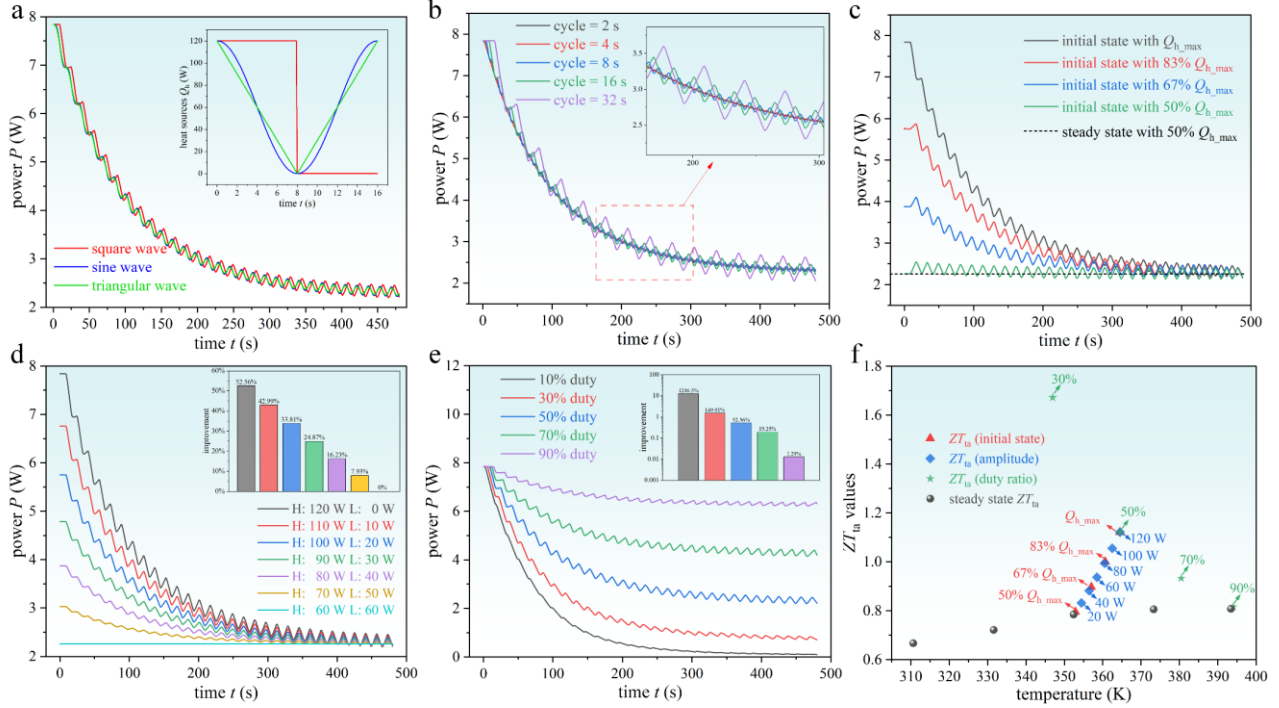29   material to the n-type one.
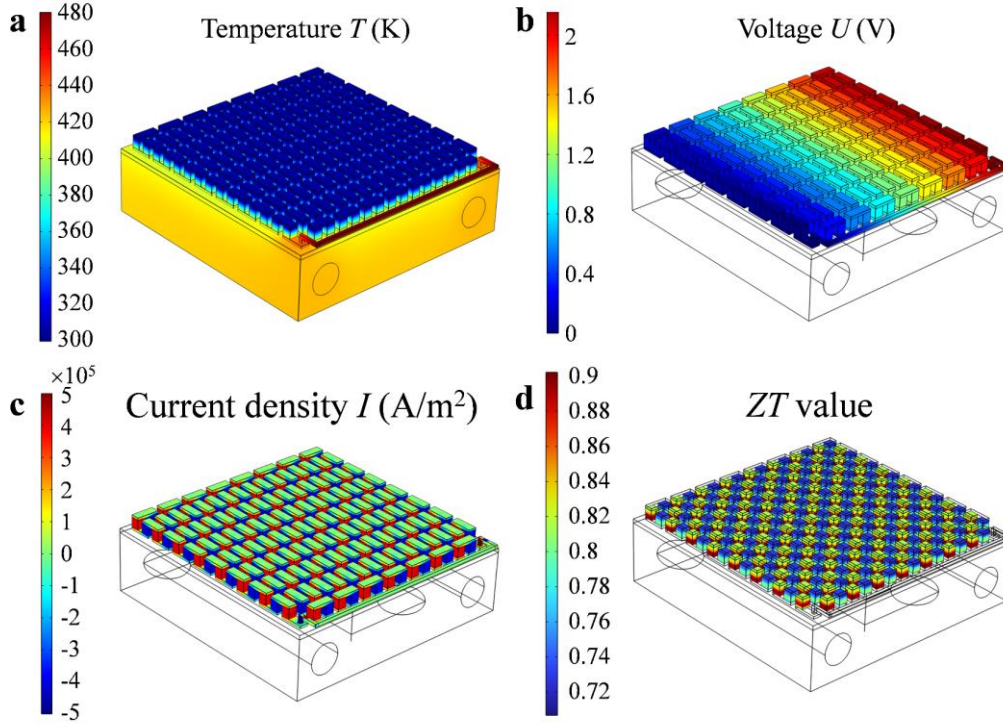
Fig. 9. 3-D distributions of the TE module with different variables. a, Steady-state temperature distributions of the TE system at $Q_h = 60$ W. **b**, Steady-state voltage distributions of the TE module at $Q_h = 60$ W. **c**, Steady-state current density distributions of the TE module at $Q_h = 60$ W. **d**, Steady-state ZT value distributions of the TE legs at $Q_h = 60$ W.

5.2 Exploration of the optimal transient heat source

The transient performance may be sensitive to the waveform, amplitude, initial state, cycle period, and duty ratio of the periodic heat source. In this regard, we studied the influences of these parameters on the dynamic behavior of the TE module. Since the TE module reaches equilibrium at $t = 480$ s, the simulation time of 480 s was adopted to perform transient simulations. We compared the dynamic power of the TE module under three periodic heat sources (Fig. 10a), including square, sine, and triangular waves. The average power under a square wave is the highest, which is 1.36% higher than the average power under a sine wave. It seems that the square wave is the best periodic heat source waveform to enhance the transient performance of the TE module, which is consistent with the analytical results in Fig. 2.

Fig. 10. Influence of different heat source parameters on the dynamic behavior of the TE module. a, Effect of the heat source waveform on the dynamic power of the TE module with a cycle period of 16 s, including square, sine, and triangular waves. **b**, Effect of the cycle period on the dynamic power of the TE module. **c**, Effect of the initial state on the dynamic power of the TE module. **d**, Effect of the amplitude on the dynamic power of the TE module. **e**, Effect of the duty ratio on the dynamic power of the TE module. **f**, ZT_{ta} values of the TE module under different heat source parameters.

Furthermore, we tried to figure out the optimal parameters of the square wave. The cycle period has little effect on the transient performance improvement, but affects the time required to reach the equilibrium state and the fluctuation amplitude of dynamic power (Fig. 10b). In principle, the cycle period shall be long enough to make the TE module reach the peak point under the excitation of positive heat source, so that the TE module can last long enough to improve performance. For instance, if the cycle period is too small, the TE module reaches the equilibrium state in a short time. This could lower the transient performance improvement level over a long time. Considering the same improvement level under different cycle periods and the optimal cycle period of 16 s for the execution time of 480 s, the cycle period of 16 s was selected in this work to illustrate the dynamic performance improvement.
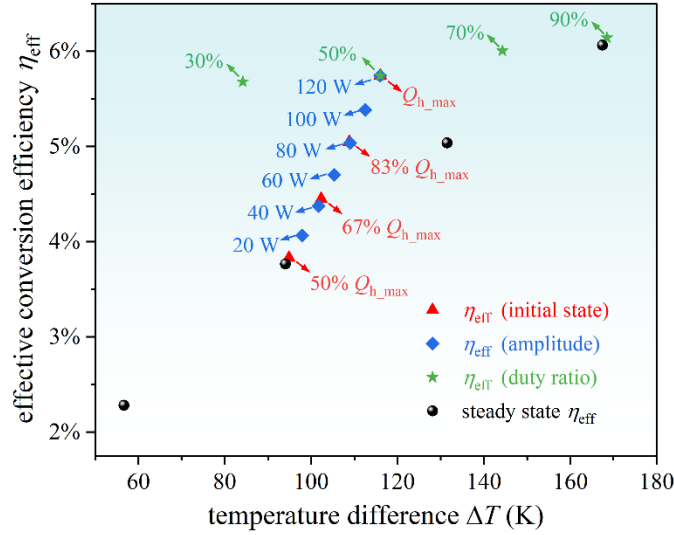
The initial thermal state of the TE module plays a significant role in the improvement of transient performance (Fig. 10c). Compared with the steady-state power with 50% Q_{h_max}, the average powers in a transient state with the initial values of 100% Q_{h_max}, 83% Q_{h_max}, 67% Q_{h_max}, and 50% Q_{h_max} increased by 52.56%, 34.10%, 18.17%, and 1.75%, respectively. Their corresponding conversion

19

1 efficiency also increases due to the same heat flux applied on the TE module in both steady and
2 transient states.

3   Similarly, the dynamic power is greatly affected by the fluctuation amplitude of the transient heat
4 source (Fig. 10d). The greater the fluctuation amplitude is, the larger the performance improvement
5 will be. As the fluctuation amplitude increases from 20 W to 120 W, the power improvement increases
6 from 7.93% to 52.56%. As a result, the TE module benefits more from operating at fluctuations in heat
7 flux between 0 W and Q_{h_max}.

8   The duty ratio is a key parameter of a square wave heat flux. A smaller duty ratio is conducive to
9 enhancing the dynamic power of the TE module within a short execution time (Fig. 10e). As the duty
10 ratio decreases from 90% to 10%, the power improvement increases from 1.29% to 1246.5%.
11 However, when the dynamic power of the TE module reaches the equilibrium state, the power excited
12 by the square wave heat source with a relatively low duty ratio is at a quite low level. To balance the
13 ability to improve the transient performance and maintain a considerable output after reaching the
14 equilibrium state, a duty ratio of 50% is suggested.

15   The conversion efficiency of the TE module is also greatly improved by periodic heating (Fig. 11).
16 Obviously, the conversion efficiency increases with the increase of temperature difference, whether in
17 a steady state or transient state. As analyzed above, the greater the initial state Q_h and fluctuation
18 amplitude are, the more obvious the improvement of the conversion efficiency is. The optimal periodic
19 heat source for the fabricated Bi_2Te_3-based TE module is the square wave with an initial state of 120
20 W, a fluctuation from 0 W to 120 W, and a duty ratio of 50%. Compared with the steady-state
21 efficiency of 3.76% at Q_h = 60 W, the conversion efficiency of the TE module under the optimal
22 periodic heat source increases by 52.56%, reaching 5.74%. According to Eq. (4), the ZT_{ta} value is also
23 greatly improved under periodic heating (Fig. 10f). Compared with the steady-state ZT_{ta} of 0.78, the
24 ZT_{ta} under the optimal periodic heat source increases by 42.95%. It reaches 1.12, which breaks the
25 limit of $ZT = 1$ for the commercial Bi_2Te_3-based TE materials at room temperature. Furthermore, the
26 ZT_{ta} value is a dimensionless constant that indicates the heat-to-electricity ability of the TE module,
27 which is lower than the ZT value of TE materials. Therefore, the ZT_{ta} value of 1.12 is equivalent to an
28 advanced TE material reaching a ZT value much higher than 1.12.

**Fig. 11.** Effective conversion efficiency η_{eff} of the TE module under different heat source parameters.

In practical applications, the heat source waveform is complex and irregular. Therefore, it is difficult to achieve a square wave. To address this issue, applying phase change materials between the heat source and TE module is a good method for regulating irregular heat sources into regular ones. In future works, we will explore an appropriate phase change material to boost the performance of TE modules in practical applications

5.3 Effect of structural and material parameters

In addition to heat source parameters, the dynamic behavior of the TE module is also affected by the interior parameters of the module, including structural and material parameters. For structural parameters, the influence of TE leg height, TE leg area, and the number of TE couples on the transient performance improvement of the TE module was investigated. The conversion efficiency increases with the increase of leg height, and the transient state η_{eff} is greater than the steady-state one (Fig. 12a). A lower height is conducive to a greater performance improvement because the transient state ZT_{ta} value decrease with the increase of leg height, and vice versa for the steady state. However, a sufficient height is necessary to ensure that the conversion efficiency of TE modules remains at a high level.

The leg area also significantly influences the transient performance of the TE module (Fig. 12b). The conversion efficiency decreases with the increase of leg area, and the transient state η_{eff} is always greater than the steady-state one. However, for the ZT_{ta} value, as the leg area increases from 0.7 mm^2 to 2.38 mm^2, the transient state ZT_{ta} increases from 0.76 to 0.79, while the steady-state ZT_{ta} decreases from 0.69 to 0.63. The periodic heat source seems more suitable for the TE module with a small leg height and a large leg area to produce a greater performance improvement. Meanwhile, the height and area should be within an appropriate range to avoid extremely low conversion efficiency.

21

Given the leg height and area, the transient performance of a TE module is greatly improved by the periodic heat source with a larger number of TE couples (Fig. 12c). Different from the previous situation where the Joule heater produced the transient heat flux, the transient heat source was directly imposed on the hot side of the TE module herein. As the number of TE couples increases, the transient state ZT_{ta} value increases greatly, but the steady state one remains unchanged. Consequently, the more TE couples contained in the TE module, the greater transient performance will be improved by periodic heating.
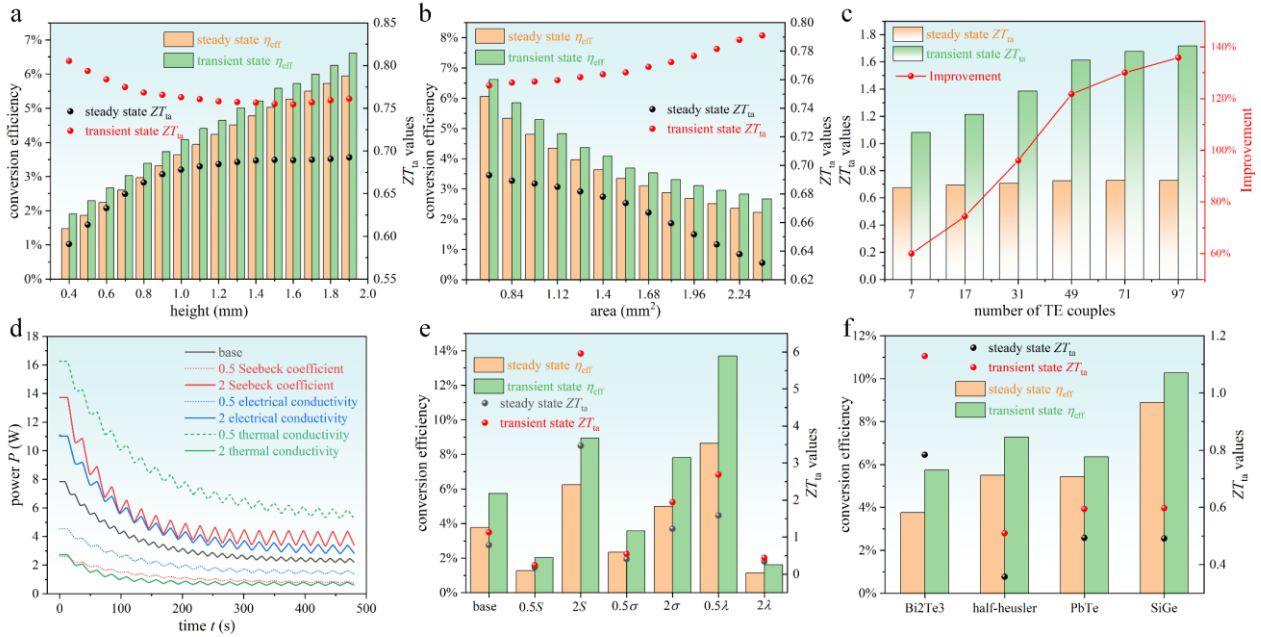
Fig. 12. Influence of structural and material parameters on the dynamic behavior of the TE module. a, Effect of the TE leg height on the improvement of conversion efficiency and ZT_{ta} value. **b**, Effect of the TE leg area on the improvement of conversion efficiency and ZT_{ta} value. **c**, Effect of the number of TE couples on the ZT_{ta} value improvement. **d**, Effect of the TE properties on the dynamic power of the TE module. **e**, Effect of the TE properties on the improvement of conversion efficiency and ZT value. **f**, Improvement of conversion efficiency and ZT_{ta} value with different kinds of TE materials.

The transient performance improvement is sensitive to TE properties. We have studied the influence of the Seebeck coefficient, electrical resistivity, and thermal conductivity on the dynamic behavior of the TE module (Fig. 12d). Here, the Bi$_2$Te$_3$-based thermoelectric properties in Table 1 were used as a benchmark. The dynamic behavior of the TE module with various Seebeck coefficient, thermal and electrical conductivity was compared. It can be seen that thermal conductivity has the greatest influence on dynamic behavior, followed by the Seebeck coefficient and electrical conductivity. This is because thermal inertia is mainly affected by thermal conductivity.

The effective conversion efficiency and average ZT_{ta} value are also influenced by the TE properties (Fig. 12e). It can be observed that the effective conversion efficiency varies greatly with TE properties,

among which the thermal conductivity presents the most influential impact. As the thermal conductivity decreases from 2 times to 0.5 times of the base, the transient effective efficiency increases from 1.63% to 13.69%. Therefore, more attention may be paid to lowering the thermal conductivity to improve the transient effective efficiency of the TE module. For the ZT_{ta} value, as the thermal conductivity decreases from 2 times to 0.5 times of the base, the steady-state ZT_{ta} value increases from 0.34 to 1.58, and the corresponding transient ZT_{ta} value increases from 0.44 to 2.68. Besides, although the Seebeck coefficient can greatly increase the ZT_{ta} value of the TE module, a relatively large improvement from the steady-state ZT_{ta} value to the transient one can also be achieved by varying the thermal conductivity.

The above-mentioned amplification effect of transient heat source on the transient performance of the TE module was studied when using different typical TE materials, including PbTe [21, 37], half-Heusler [19, 38], and SiGe [39, 40] based materials. Here, the geometric parameters of TE modules with different materials are identical. Considering the optimal working temperatures for the three materials are different, the maximum supplied heat (Q_{max}) for the PbTe, half-Heusler, and SiGe-based TE modules was set as 180 W, 650 W, and 600 W, respectively. Under the heat supply of square wave heat source, the conversion efficiency of PbTe, half-Heusler, and SiGe-based TE modules was increased from 5.43%, 5.50%, and 8.89% under steady state to 6.36%, 7.28%, and 10.27% under transient state, respectively. The corresponding ZT_{ta} values increased from 0.49, 0.36, and 0.49 to 0.59, 0.51, and 0.60, respectively. It can be concluded that the transient performance improvement of the Bi_2Te_3-based TE module is obviously higher than that based on the other three materials. This is probably because the geometric parameters used are optimal for the Bi_2Te_3-based TE module but not for the modules based on other materials. This could cause a great impact as geometric parameters have a significant influence on the dynamic behavior of the TE module (Figs 12a-c).

6. Conclusions

In this study, we disclose a periodic heating method to improve the dynamic behavior of the TE module. To accurately estimate the dynamic behavior of the TE module in practical transient applications, two new indicators, time average ZT_{ta} value and effective conversion efficiency, are proposed. A Bi_2Te_3-based TE module with n-type $Bi_2Te_{3-x}Se_x$ and p-type $Bi_xSb_{2-x}Te_3$ materials is manufactured and used as the research objective. Besides, a transient experimental bench is designed to validate the effectiveness of the periodic heating method in improving the dynamic performance, and the thermal and electrical contact resistances of the TE module are measured. To explore the optimal heat source and study the effect of different parameters on the dynamic behavior, a 3D transient

thermal-electric numerical is also developed. Through experiments and numerical simulations, the following conclusions are obtained:

(1) Based on experimental results, the interior thermal contact resistance, hot-side and cold-side thermal contact resistances of the TE module are 3.65×10^{-5} m$^2 \cdot$K/W, 1.78×10^{-4} m$^2 \cdot$K/W, and 1.39×10^{-4} m$^2 \cdot$K/W, respectively, and the electrical contact resistance is $1.18 \times 10^{-10} \Omega \cdot$ m^2. Besides, the developed 3D transient thermal-electric numerical model is well-verified experimentally.

(2) At a heat supply of 60 W, the TE module reaches a conversion efficiency of 3.76% and ZT_{ta} value of 0.78 in a steady state, while the effective conversion efficiency and ZT_{ta} value reach 5.75% and 1.12 in a transient state (a square wave with a duty cycle of 50% and a period of 16 s fluctuates between 120 W and 0 W), improved by 52.93% and 43.59% respectively. In addition, from the perspective of material optimization, attaining a ZT_{ta} value of 1.12 implies the requirement for an advanced TE material capable of exceeding a ZT value of much higher than 1.12.

(3) In practical applications, the heat source fluctuates frequently, and it is necessary to use the developed transient indicators to estimate the performance of the TE module. Compared with steady conversion efficiency calculated through average values, the effective conversion efficiency is more accurate in evaluating the dynamic behavior of the TE module. Compared with the ZT value of thermoelectric materials, the time average ZT_{ta} value can reflect the heat-to-electricity conversion ability over the entire specific transient cycle from a module level.

(4) The material and structural parameters of the TE module play a significant role in the dynamic behavior. For structural parameters, a smaller leg height, a larger leg area, and more TE couples are conducive to improving the dynamic performance of the TE module, while for material parameters, more attention should be paid to lowering the thermal conductivity of thermoelectric materials.

(5) The proposed periodic heating method provides a new route toward the performance improvement of TE modules, which may promote the broader applications of thermoelectric power generation technology. In practical applications, considering the irregular changes in the heat source, applying phase change materials to the hot side of the TE module is able to obtain the desired periodic heat source, and the corresponding studies will be performed in our future studies.

References

[1] Rowe DM. Thermoelectrics handbook: macro to nano: CRC press; 2005.

[2] Kishore RA, Nozariasbmarz A, Poudel B, Sanghadasa M, Priya S. Ultra-high performance wearable thermoelectric coolers with less materials. Nature Communications. 2019;10:1765.

[3] Zhang Y. Thermoelectric Advances to Capture Waste Heat in Automobiles. ACS Energy Letters. 2018;3:1523-4.

[4] Luo D, Sun Z, Wang R. Performance investigation of a thermoelectric generator system applied in automobile exhaust waste heat recovery. Energy. 2022;238:121816.

[5] Luo D, Yan Y, Chen W-H, Yang X, Chen H, Cao B, et al. A comprehensive hybrid transient CFD-thermal resistance model for automobile thermoelectric generators. Int J Heat Mass Transfer 2023;211:124203.

[6] Miao Z, Meng X, Liu L. Improving the ability of thermoelectric generators to absorb industrial waste heat through three-dimensional structure optimization. Appl Therm Eng 2023;228:120480.

[7] Wang C, Tang S, Liu X, Su GH, Tian W, Qiu S. Experimental study on heat pipe thermoelectric generator for industrial high temperature waste heat recovery. Appl Therm Eng 2020;175:115299.

[8] Nour Eddine A, Chalet D, Faure X, Aixala L, Chessé P. Optimization and characterization of a thermoelectric generator prototype for marine engine application. Energy. 2018;143:682-95.

[9] Georgopoulou CA, Dimopoulos GG, Kakalis NMP. A modular dynamic mathematical model of thermoelectric elements for marine applications. Energy. 2016;94:13-28.

[10] Zhang Q, Liao J, Tang Y, Gu M, Ming C, Qiu P, et al. Realizing a thermoelectric conversion efficiency of 12% in bismuth telluride/skutterudite segmented modules through full-parameter optimization and energy-loss minimized integration. Energy Environ Sci 2017;10:956-63.

[11] Wang X, Wang H, Su W, Chen T, Tan C, Madre MA, et al. U-type unileg thermoelectric module: A novel structure for high-temperature application with long lifespan. Energy. 2022;238:121771.

[12] Crane DT, Lagrandeur JW, Harris F, Bell LE. Performance Results of a High-Power-Density Thermoelectric Generator: Beyond the Couple. J Electron Mater 2009;38:1375-81.

[13] Luo D, Wang R, Yu W, Zhou W. A numerical study on the performance of a converging thermoelectric generator system used for waste heat recovery. Appl Energy 2020;270:115181.

[14] Bai W, Yuan X, Liu X. Numerical investigation on the performances of automotive thermoelectric generator employing metal foam. Appl Therm Eng 2017;124:178-84.

[15] Pacheco N, Brito FP, Vieira R, Martins J, Barbosa H, Goncalves LM. Compact automotive thermoelectric generator with embedded heat pipes for thermal control. Energy. 2020;197:117154.

1 [16] Jung YS, Jeong DH, Kang SB, Kim F, Jeong MH, Lee K-S, et al. Wearable solar thermoelectric
2   generator driven by unprecedentedly high temperature difference. Nano Energy. 2017;40:663-72.
3 [17] Suarez F, Nozariasbmarz A, Vashaee D, Öztürk MC. Designing thermoelectric generators for
4   self-powered wearable electronics. Energy Environ Sci 2016;9:2099-113.
5 [18] LaLonde AD, Pei Y, Wang H, Jeffrey Snyder G. Lead telluride alloy thermoelectrics. Mater
6   Today 2011;14:526-32.
7 [19] Liu Y, Fu C, Xia K, Yu J, Zhao X, Pan H, et al. Lanthanide Contraction as a Design Factor for
8   High-Performance Half-Heusler Thermoelectric Materials. Adv Mater 2018;30:1800881.
9 [20] Ahmad S, Singh A, Bohra A, Basu R, Bhattacharya S, Bhatt R, et al. Boosting thermoelectric
10   performance of p-type SiGe alloys through in-situ metallic YSi2 nanoinclusions. Nano Energy.
11   2016;27:282-97.
12 [21] Ohta M, Biswas K, Lo S-H, He J, Chung DY, Dravid VP, et al. Enhancement of Thermoelectric
13   Figure of Merit by the Insertion of MgTe Nanostructures in p-type PbTe Doped with Na2Te.
14   Advanced Energy Materials. 2012;2:1117-23.
15 [22] Bell LE. Cooling, Heating, Generating Power, and Recovering Waste Heat with Thermoelectric
16   Systems. Science. 2008;321:1457.
17 [23] Poudel B, Hao Q, Ma Y, Lan Y, Minnich A, Yu B, et al. High-thermoelectric performance of
18   nanostructured bismuth antimony telluride bulk alloys. Science. 2008;320:634-8.
19 [24] Kim SI, Lee KH, Mun HA, Kim HS, Hwang SW, Roh JW, et al. Dense dislocation arrays
20   embedded in grain boundaries for high-performance bulk thermoelectrics. Science.
21   2015;348:109-14.
22 [25] Zhuang H-L, Hu H, Pei J, Su B, Li J-W, Jiang Y, et al. High ZT in p-type thermoelectric
23   (Bi,Sb)2Te3 with built-in nanopores. Energy Environ Sci 2022;15:2039-48.
24 [26] Luo D, Yan Y, Wang R, Zhou W. Numerical investigation on the dynamic response characteristics
25   of a thermoelectric generator module under transient temperature excitations. Renewable Energy
26   2021;170:811-23.
27 [27] Apostol M, Nedelcu M. Pulsed thermoelectricity. J Appl Phys 2010;108.
28 [28] Gray PE, Wolfe R. The Dynamic Behavior of Thermoelectric Devices. J Electrochem Soc
29   1960;107:242C.
30 [29] Sun Z, Luo D, Wang R, Li Y, Yan Y, Cheng Z, et al. Evaluation of energy recovery potential of
31   solar thermoelectric generators using a three-dimensional transient numerical model. Energy.
32   2022;256:124667.

[30] Yee SK, LeBlanc S, Goodson KE, Dames C. $ per W metrics for thermoelectric power generation: beyond ZT. Energy Environ Sci 2013;6:2561-71.

[31] Zhao D, Tan G. A review of thermoelectric cooling: Materials, modeling and applications. Appl Therm Eng 2014;66:15-24.

[32] Hao F, Qiu P, Tang Y, Bai S, Xing T, Chu H-S, et al. High efficiency Bi2Te3-based materials and devices for thermoelectric power generation between 100 and 300 °C. Energy Environ Sci 2016;9:3120-7.

[33] Yan Y, Malen JA. Periodic heating amplifies the efficiency of thermoelectric energy conversion. Energy Environ Sci 2013;6:1267-73.

[34] Xu G, Duan Y, Chen X, Ming T, Huang X. Effects of thermal and electrical contact resistances on the performance of a multi-couple thermoelectric cooler with non-ideal heat dissipation. Appl Therm Eng 2020;169:114933.

[35] Esfahani JA, Rahbar N, Lavvaf M. Utilization of thermoelectric cooling in a portable active solar still — An experimental study on winter days. Desalination. 2011;269:198-205.

[36] Delfani F, Rahbar N, Aghanajafi C, Heydari A, KhalesiDoost A. Utilization of thermoelectric technology in converting waste heat into electrical power required by an impressed current cathodic protection system. Appl Energy 2021;302:117561.

[37] Androulakis J, Lin C-H, Kong H-J, Uher C, Wu C-I, Hogan T, et al. Spinodal Decomposition and Nucleation and Growth as a Means to Bulk Nanostructured Thermoelectrics: Enhanced Performance in Pb1-xSnxTe−PbS. JACS 2007;129:9780-8.

[38] Yu J, Fu C, Liu Y, Xia K, Aydemir U, Chasapis TC, et al. Unique Role of Refractory Ta Alloying in Enhancing the Figure of Merit of NbFeSb Thermoelectric Materials. Advanced Energy Materials. 2018;8:1701313.

[39] Joshi G, Lee H, Lan Y, Wang X, Zhu G, Wang D, et al. Enhanced Thermoelectric Figure-of-Merit in Nanostructured p-type Silicon Germanium Bulk Alloys. Nano Lett 2008;8:4670-4.

[40] Wang XW, Lee H, Lan YC, Zhu GH, Joshi G, Wang DZ, et al. Enhanced thermoelectric figure of merit in nanostructured n-type silicon germanium bulk alloy. Appl Phys Lett 2008;93:193121.